Updated Cosmology

with Python

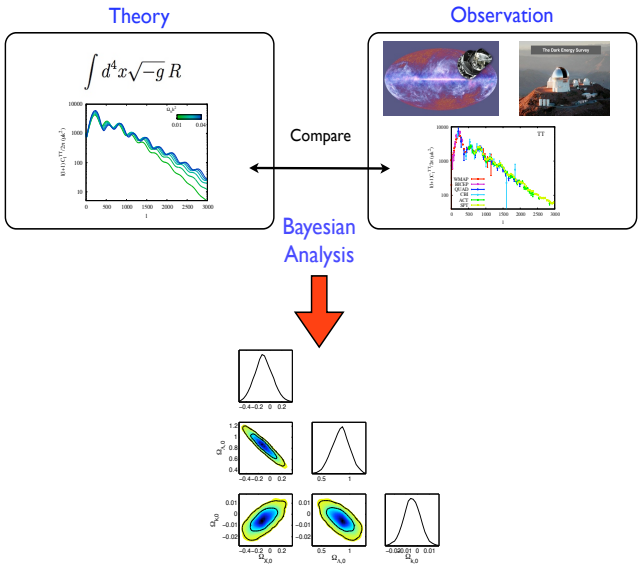

José-Alberto Vázquez

ICF-UNAM / Kavli-Cambridge

In progress

August 12, 2017

1

Statistics in Cosmology

In the previous chapter we have developed the main equations to describe the evolution of the background and perturbed universe. We noticed, however, that the whole structure of the CMB, matter power spectrum and luminosity distance depend strongly on the initial conditions emerging from the inflationary era ($\mathcal{P}_{\mathcal{R},\mathcal{T}}$), on the matter-energy content ($\Omega_{i,0}$), and on the expansion rate history (H_0). This chapter seeks to give a brief introduction of such quantities used to describe the properties of the universe. We show current and future experimental results used throughout the analysis: CMB, SNe and LSS amongst many others. It also includes a short description of the Bayesian analysis to perform the parameter estimation and model selection. Finally, at the end of the chapter, by making use of the theoretical, observational and statistical tools included in this work, we examine the standard ΛCDM model (spatially flat and non-flat), and present the current constraints on the cosmological parameters.

1.1 The Cosmological Parameters

1.1.1 Base parameters

These parameters, commonly called *standard parameters*, are considered as the principal quantities used describe the universe. They are not, however, predicted by any fundamental theory, rather we have to fit them by hand in order to determine which combination best describes the current astrophysical observations [34, 38]. Variations of these parameters affect the amplitude and shape of the spectra as well as the background evolution in many different ways, yielding to very different universes. They are classified depending on whether they characterise the background or the perturbed universe:

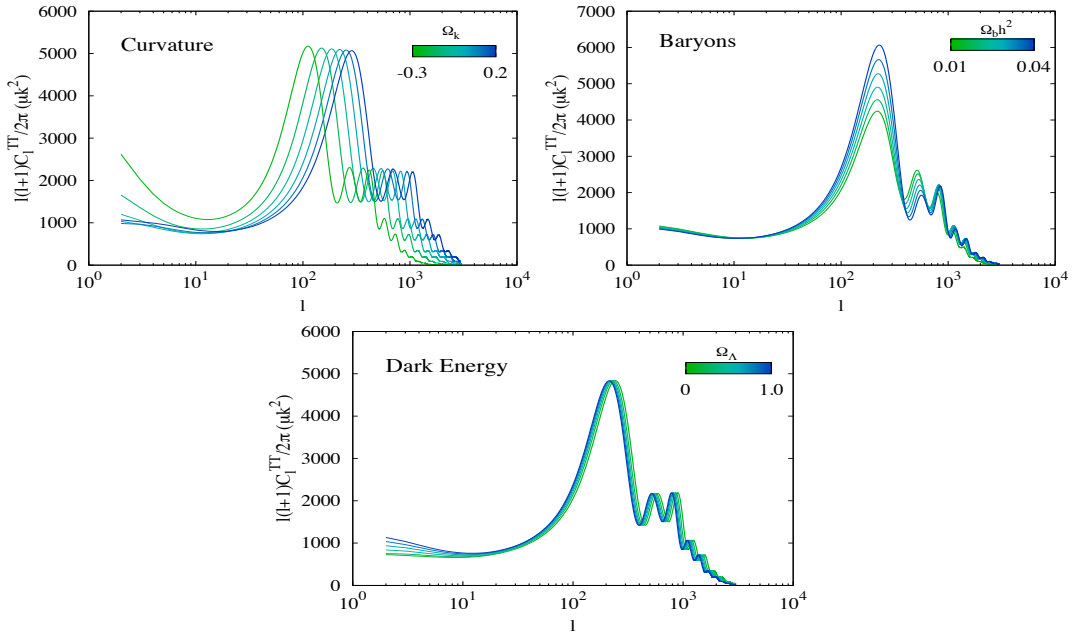

Figure 1.1: Dependence of the temperature power spectrum for three fundamental quantities: Curvature (Ω_k), Baryons (Ω_b) and Dark energy in the form of a cosmological constant (Ω_Λ).

Background parameters

The present description of the homogeneous universe can be given in terms of the density parameters $\Omega_{i,0}$ and the Hubble parameter H_0, through the Friedmann equation (**??**):

$$H^2 = H_0^2 \left[(\Omega_{\gamma,0} + \Omega_{\nu,0})\, a^{-4} + (\Omega_{\mathrm{b},0} + \Omega_{\mathrm{dm},0})\, a^{-3} + \Omega_{k,0} a^{-2} + \Omega_{X,0} a^{-1} + \Omega_{\Lambda,0} \right], \qquad (1.1)$$

From these parameters the radiation contribution is accurately measured, for instance by the WMAP satellite, corresponding to $\Omega_{\gamma,0} = 2.469 \times 10^{-5} h^{-2}$ for $T_\mathrm{cmb} = 2.725K$. Similarly for neutrinos, while taken as relativistic, they can be related to the photon density through (**??**). However, variations of the rest of the parameters imprint different signatures on the background history and evolution of perturbations, observed through the CMB spectrum as it is illustrated in Figure 1.1. We observe that the first peak (and the most prominent, at $l \approx 200$) is particularly related to the spatial geometry $\Omega_{k,0}$; the relative heights of the intermediate peaks probe the baryon density; the largest scales are mainly affected by the dark energy component.

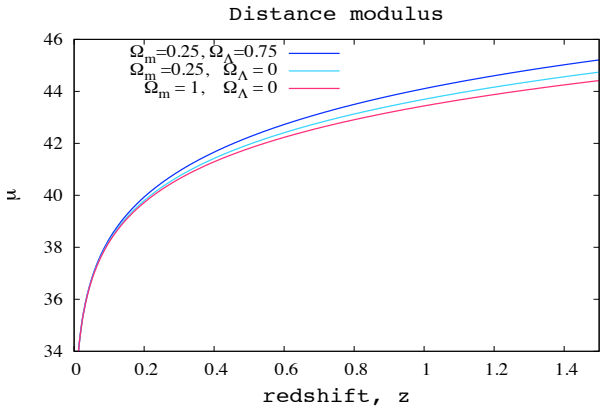

Figure 1.2: Theoretical values of the distance modulus μ for three different models; with various combinations of matter $\Omega_{m,0}$ and dark energy in the form of a cosmological constant $\Omega_{\Lambda,0}$.

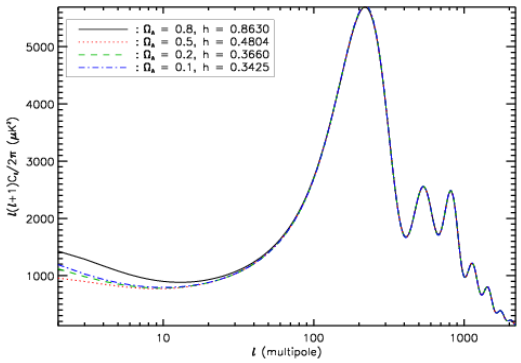

Figure 1.3: Cosmic Degeneracy

These base parameters also play a key role on measurements of the distance modulus μ, through the luminosity distance (**??**). Figure 1.2 shows the theoretical values of the distance modulus for three different models with various combinations of $\Omega_{m,0}$ and $\Omega_{\Lambda,0}$. Note that objects appear to be further away (dimmer) in a universe with cosmological constant than one dominated by only matter today.

The existence of strong degeneracies amongst different combinations of parameters is also noticeable. In particular the well-known *geometrical degeneracy* involving Ω_m, Ω_Λ and the curvature parameter $\Omega_k = 1 - \Omega_m - \Omega_\Lambda$.

To reduce degeneracies it is common to introduce a combination of the cosmological pa-

rameters such that they have orthogonal effects on the power spectrum [32]. For instance, a standard parameterisation is based on the *physical energy-densities* of cold dark matter $\Omega_{\rm dm}h^2$, and baryons $\Omega_{\rm b}h^2$, and the ratio of the sound horizon to the angular diameter distance at decoupling time:

$$\theta = \frac{r_{\rm s}(a_{\rm dec})}{D_A(a_{\rm dec})}. \tag{1.2}$$

There is an extra parameter that accounts for the reionisation history of the universe, the *optical depth to scattering* τ (i.e. the probability that a given photon scatters once), given by

$$\tau = \sigma_{\rm T} \int_{t_r}^{t_0} n_e(t) dt, \tag{1.3}$$

where $\sigma_{\rm T}$ is the Thompson cross-section and $n_e(t)$ is the electron number density as a function of time.

Inflationary parameters

After the horizon exit, H and $\dot{\phi}$ have small variations during few e-folds. Thus, the scalar (**??**) and tensor (**??**) spectra are nearly scale independent. The standard assumption is therefore to parameterise each of the spectra in terms of a power-law

$$\mathcal{P}_{\mathcal{R}}(k) = A_{\rm s} \left(\frac{k}{k_0}\right)^{n_{\rm s}-1}, \tag{1.4}$$

$$\mathcal{P}_{\mathcal{T}}(k) = A_{\rm t} \left(\frac{k}{k_0}\right)^{n_{\rm t}}. \tag{1.5}$$

where $A_{\rm s}$, $A_{\rm t}$ are the *spectral amplitudes*, and $n_{\rm s}$, $n_{\rm t}$ the *spectral indices* or *tilt parameters*, for both scalar and tensor perturbations respectively; k_0 denotes an arbitrary scale at which the tilted spectrum pivots, usually fixed to $k_0 = 0.002$ Mpc^{-1}. A scale-invariant spectrum, called Harrison-Zel'dovich (HZ), has constant variance on all length scales and it is characterised by $n_{\rm s} = 1$, $n_{\rm t} = 0$. Small deviations from scale-invariance are also considered as typical signatures of inflationary models [40]. The spectrum of perturbations is said to be blue if $n_{\rm s} > 0$ (more power in ultraviolet), and red if $n_{\rm s} < 0$ (more power in infrared). The spectral indices, $n_{\rm s}$ and $n_{\rm t}$, and the tensor-to-scalar ratio r can be expressed in terms of the slow-roll parameters $\epsilon_{\rm v}$ and $\eta_{\rm v}$ (**??**), as:

$$n_{\rm s} - 1 \simeq -6\,\epsilon_{\rm v}(\phi) + 2\,\eta_{\rm v}(\phi), \tag{1.6}$$

$$n_{\rm t} \simeq -2\,\epsilon_{\rm v}(\phi), \tag{1.7}$$

$$r \simeq 16\,\epsilon_{\rm v}(\phi). \tag{1.8}$$

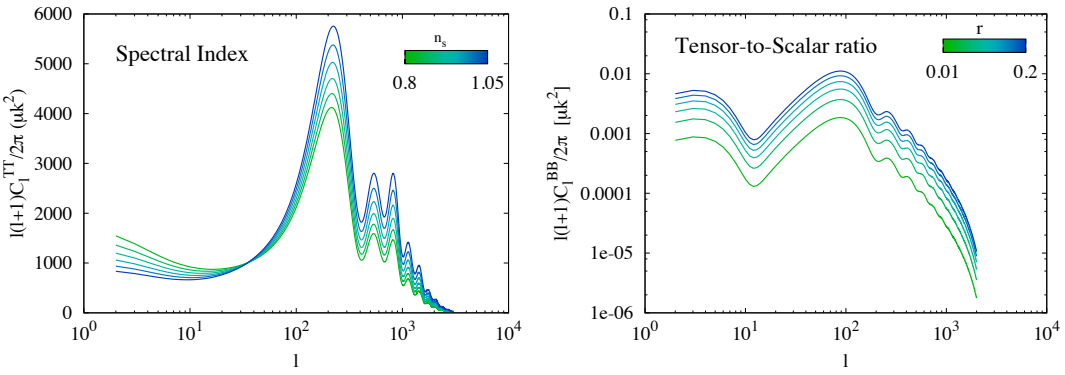

Figure 1.4: Variations of the C^{TT} scalar spectrum for different values of the spectral index n_s (left), and variations of the C^{BB} tensor spectrum with respect to the tensor-to-scalar ratio r (right).

These parameters are not completely independent each other, but the tensor spectral index is proportional to the tensor-to-scalar ratio $r = -8n_{\rm t}$ [12]. This expression is considered as the *consistency relation* for slow-roll inflation. Any single-field inflationary model can hence be described, to the lowest order in slow-roll, in terms of three independent parameters: the amplitude of density perturbations $A_{\rm s}$, the scalar spectral index $n_{\rm s}$, and the tensor-to-scalar ratio r. Variations of the CMB T-spectrum over different values of $n_{\rm s}$ are shown in the left panel of Figure 1.4.

In addition to the temperature T and polarisation E spectra, produced by scalar perturbations, there is also the B-mode polarisation only produced by tensor perturbations. Therefore, measurements of B-modes are important tests for the existence of primordial gravitational waves. Unfortunately, there is no observational evidence of tensor perturbations yet, and r is commonly set to zero. The next generation of CMB polarisation experiments will substantially improve these limits (see Section 1.2.2). Variations of the C^{BB} tensor spectrum with respect to the tensor-to-scalar ratio r are displayed in the right panel of Figure 1.4.

1.1.2 Nuisance parameters

We do not have particular interest on these type of parameters, however they may influence the rest of the parameter-space constraints. These type of parameters may be related to insufficiently constrained aspects of physics, or uncertainties in the measuring process [**?**]. Therefore,

considering their uncertainty is important in order to obtain accurate error-estimates on the physical parameters we are seeking to determine. Examples of nuisance parameters are, for instance, the bias factor in galaxy surveys b, calibrations and beams uncertainties, galactic foregrounds. The new ACT measurements (three seasons of data [59]) incorporate nine parameters describing secondary emissions. Nuisance parameters also control the stretch α and colour β corrections on measurements of distance modulus of SNe Type Ia [43].

1.1.3 Derived parameters

The standard set of parameters, introduced previously, provide an adequate description of the cosmological models in agreement with observational data. However, it is not unique and other parameterisations may be as good as this one. Some parameterisations make use of knowledge about physics or sensitivity of observations and are hence more naturally interpreted. In general we could have used different parameters to describe the universe, those include: the age of the universe, the present neutrino background temperature, the epoch of matter-radiation equality, the reionisation epoch, the baryon to dark matter density ratio, or some other combinations of parameters, i.e. the overall amplitude of the CMB anisotropy $\exp(-2\tau)A_{\rm s}$ [**?**]. In the ΛCDM model, to ameliorate degeneracies, we use as base parameters the physical energy densities $\Omega_{\rm dm,0}h^2$ and $\Omega_{\rm b,0}h^2$, and the ratio of the sound horizon to the angular diameter distance θ; we consider as derived quantities the density parameters $\Omega_{i,0}$ and Hubble parameter H_0.

1.1.4 Beyond the concordance ΛCDM

The best model in agreement with data, at present time, is given by the concordance ΛCDM model. However, this model might not be the final one and several extensions have already been implemented. A non-exhaustive list of candidates beyond the standard cosmological model is shown in Table 1.1. The definite answer on how many parameters we must include or which set of parameters represents the most plausible will be given by high-quality cosmological observations in the coming years. In the same table, we have highlighted the models studied in detail throughout this work.

1.2 Observations

Rapid advance in the development of powerful observational-instruments has led to the establishment of *precision cosmology*. In particular, experiments employed to measure CMB

Table 1.1: Candidate parameters used to describe models beyond the concordance ΛCDM. The highlighted models are studied in detail throughout this work.

αR^n	Modifications to gravity
	[or more complex theories]
$d\tilde{s}^2$	Anisotropic universe
$d\alpha/dz$, dG/dz	Variations of fundamental constants
$f_{\rm NL}$	Non-gaussianity
$n_{\rm run}$	Running of the scalar spectral index
$k_{\rm cut}$	Large-scale cut-off in the spectrum
	[or a more complex parameterisation of $\mathcal{P}_\mathcal{R}(k)$]
$r + 8n_{\rm t}$	Violation of the inflationary consistency relation
$n_{\rm t,run}$	Running of the tensor spectral index
	[or a more complex parameterisation of $\mathcal{P}_\mathcal{T}(k)$]
$P_{\rm iso}$	CDM isocurvature perturbations
$\Omega_{k,0}$	Spatial curvature
$\Omega_{X,0}$	Additional components
$m_{\rm dm}$	Warm dark matter mass
	[or scalar field dark matter]
m_{ν_i}	Neutrino mass for species 'i'
$w_{\rm DE}$	Dark energy equation-of-state
	[or a more complex parameterisation of $w(z)$]
ρ^α	Polytropic equation of state
Γ	Interacting fluids

anisotropies, luminosity distances and large-scale structure. In this section, we highlight these type of experiments used to impose constraints on the cosmological parameters.

1.2.1 Current observations

CMB experiments

A number of experiments over the past decade or so have been very successful in measuring the anisotropies of the CMB. They include the Cosmic Background Explorer satellite [COBE; 45] as the pioneer of detecting the anisotropy. Nowadays with highly-improved experiments it is possible to find accurate measurements of the temperature and polarisation CMB spectrum from:

Satellite experiments:

- The Wilkinson Microwave Anisotropy Probe [WMAP; 31, 35], with CMB T-spectrum measurements over the multipoles ($2 < l < 1200$). Recently the WMAP collaboration has released the 9-year of observations [22].

Ground-based telescopes:

- The Background Imaging of Cosmic Extragalactic Polarization [BICEP; 11], probes intermediate scales ($21 \leq l \leq 335$).
- The Quest (Q and U Extra-Galactic Sub-mm Telescope) at DASI (Degree Angular Scale Interferometer) [QUAD; 9], improve polarisation constraints, whose primary aim is high resolution measurements ($154 \leq l \leq 2026$) of the polarisation signals.
- The Cosmic Background Imager [CBI; 60], constrains the CMB spectrum in the range ($300 \leq l \leq 1700$).
- The Atacama Cosmology Telescope [ACT; 15], observes the small angle CMB T-spectrum from l= 300 to l=10000, and recently released the three seasons of data [59].
- The South Pole Telescope [SPT; 29], with CMB T-measurements between ($650 < l < 9500$), and recent improved data from the 2500-square-degree SPT-SZ survey [63].

Ballon-borne experiments:

- Balloon Observations Of Millimetric Extragalactic Radiation AND Geophysics [BOOMERanG; 28], measures CMB temperature fluctuations over the multipole range $50 \leq l \leq 1500$.

Figure 1.5 summarises the current status of some experiments constraining the temperature (TT), polarisation (EE) and cross-correlation (T-E) CMB power spectra. In particular the CMB T-power spectrum is now well-constrained over a wide range of scales. For example, WMAP and BICEP observations provide good constraints on the late-time ISW effect arising at the largest scales on the first three acoustic peaks, whilst ACT and SPT data accurately measure the power of higher acoustic peaks and damping tail. Intermediate scales are well constrained by QUAD and CBI experiments, and the overlapping of all of them. In addition to T, E and T-E CMB spectra, Figure 1.6 shows the theoretical B-mode spectrum predicted from a power-law parameterisation, with $r = 0.1$, along with 1σ constraints obtained from

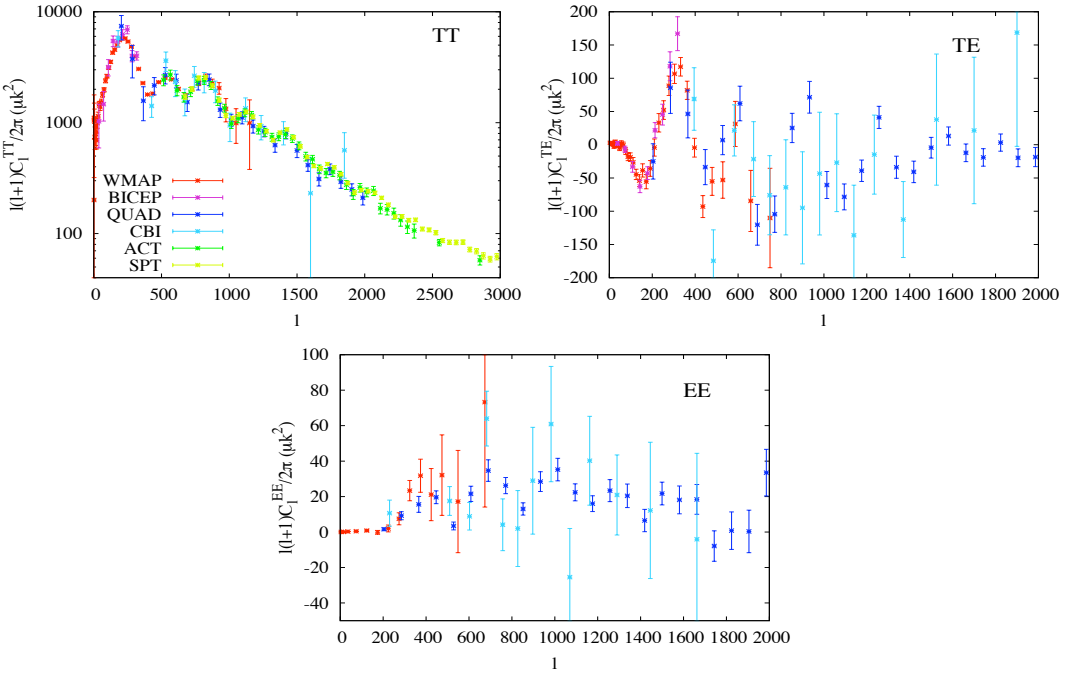

Figure 1.5: Current status of temperature (TT), polarisation (EE) and cross-correlation (T-E) measurements of the CMB power spectra, by various observational probes.

current observations: WMAP, BICEP and QUAD.

At this point it is worthwhile mentioning the existence of an intrinsic uncertainty in the cosmological measurements. This limitation comes from the fact that we have to do statistics with only one universe. For a given multipole l, we expect to have a variance, called the *cosmic variance*, of the C_l's given by

$$(\Delta C_l)^2 = \frac{2}{2l+1} C_l^2. \tag{1.9}$$

In real experiments, the error is increased due to the limited sky coverage by f_{sky}^{-1}.

CMB measurements by themselves cannot, however, place strong constraints on all the parameters because the existence of parameter degeneracies, such as the $\tau - A_s$ and the geometrical degeneracy. Nevertheless, when CMB observations are combined with other cosmological probes, they together increase the constraining power and considerably weaken degeneracies.

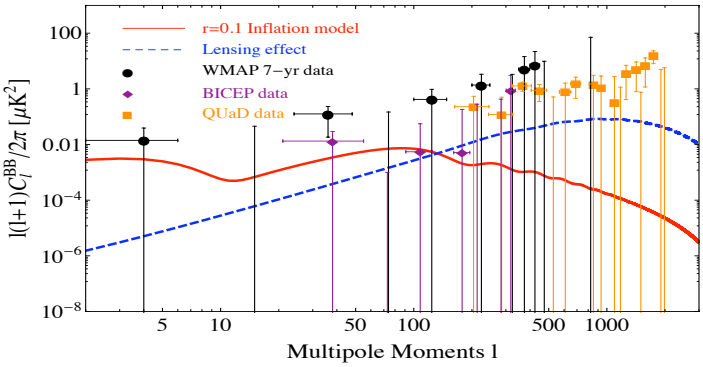

Figure 1.6: WMAP, BICEP and QUaD constraints for the B-mode power spectrum. The solid line represents the theoretical prediction of a $r = 0.1$.

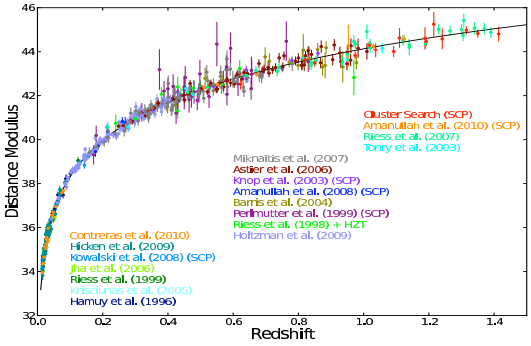

Figure 1.7: Current status of measurements of the Hubble diagram of Type Ia supernovae. Reprinted from the Union 2.1 compilation [65].

Supernovae observations

Throughout the past two decades supernovae observations have provided decisive evidence that the present expansion of the universe is accelerating. In particular studies of Type Ia supernovae as standard candles: they have the same intrinsic magnitude with high accuracy, up to a rescaling factor, e.g. Perlmutter et al. [50], Riess et al. [57]. Hence, the current acceleration suggests the existence of an exotic component or alternative theories which would produce such an effect, as we will see in Chapters **??** and **??**. Branch and Tammann [7] provides a brief introduction to Type Ia supernovae (SNe Ia) as standard candles, and **?**] shows their use in cosmology. Some samples of supernovae Type Ia worth mentioning include:

- The Sloan Digital Sky Survey-II [SDSS-II; 19], discovered and measured multi-band

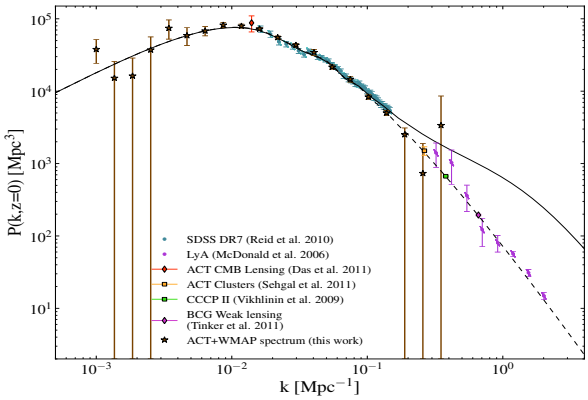

Figure 1.8: Current status of the perturbation power spectrum as measured by different experiments. Figure reproduced from [23].

lightcurves for 327 spectroscopically confirmed Type Ia supernovae in the redshift range $0.05 < z < 0.35$.

- The Equation of State: SupErNovae trace Cosmic Expansion program [ESSENCE; 47], discovered and analysed 60 Type Ia supernovae over the redshift interval $0.15 < z < 0.70$,
- The Supernova Legacy Survey 3-year sample [SNLS; 64], presented 252 high redshift Type Ia supernovae ($0.15 < z < 1.1$).
- The Hubble Space Telescope [HST; 55], discovered 21 Type Ia supernovae at $z \geq 1$.
- Recently the compilation of data from all the above, namely the 'Union' [33], 'Union 2' [3] and 'Union 2.1' [65].

Supernovae measurements can be plotted on a Hubble diagram with distance modulus vs. redshift (as seen in Figure 1.7), and then be used to fit the best cosmological parameters, for instance those shown in Figure 1.2.

LSS measurements

The matter power spectrum is nowadays one of the most important measures of large-scale structure. Many observations have been made to infer the spectrum:

- The sample of Luminous Red Galaxies (LRGs) from the Sloan Digital Sky Survey Seventh Data Release (DR7) [54], provides measurements on the matter spectrum between $0.02 <$

$k < 0.19\text{Mpc}^{-1}$. Nowadays with improved measurements, one has the ninth data released (DR9) of the SDSS-III [1].

- Measurements of the transmitted flux in the Lyα forest probe the smallest scales in the matter power spectrum [46].

An illustration of the matter power spectrum of density fluctuations is shown in Figure 1.8 (see [23] and references therein).

1.2.2 Future surveys

An impressive array of ambitious projects have been implemented, or are underway, to provide high resolution measurements of the physical properties of the universe, and hence the search for possible signatures of new cosmology. The Planck satellite [52] will improve measurements on the E and B polarisation modes. Along with Planck satellite there will be several experiments aiming to provide measurements of small-scale fluctuations and polarisations, such as the E and B EXperiment [EBEX; 49], Q-U-I JOint TEnerife CMB experiment [QUIJOTE; 58] and Spider [13]. Besides CMB experiments, the Euclid satellite [16] will explore the expansion history of the universe and the evolution of cosmic structures over a very large fraction of the sky. The Dark Energy Survey [DES; 66] is designed to probe the origin of the accelerating universe and help uncover the nature of dark energy.

Previously we have shown current constraints of the temperature and polarisation CMB spectra. Here, we aim to explore future constraints coming from Planck satellite and CMB-Pol experiments. Performance assumptions for Planck and CMB-Pol are taken from [52] and [5]. In order to do this we need to simulate these experiments by generating mock data of the $\hat{C}_l^{XY}$'s from a χ^2_{2l+1} distribution with variances [53]:

$$(\Delta\hat{C}_l^{XX})^2 = \frac{2}{(2l+1)f_{sky}}\left(C_l^{XX}+N_l^{XX}\right)^2, \tag{1.10}$$

$$(\Delta\hat{C}_l^{TE})^2 = \frac{2}{(2l+1)f_{sky}}\left[\left(C_l^{TE}\right)^2+\left(C_l^{TT}+N_l^{TT}\right)\left(C_l^{EE}+N_l^{EE}\right)\right], \tag{1.11}$$

where $X = T, E$ and B label the temperature and polarisations; f_{sky} is the fraction of the observed sky. The C_l^{XY}'s represent the theoretical spectra and N_l^{XY} the instrumental noise spectra for each experiment. In experiments with multiple frequency channels c, the noise spectrum is approximated [6] by

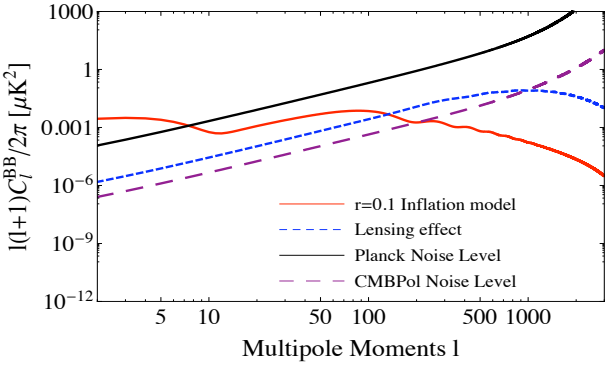

Figure 1.9: Polarisation noise power spectra of forthcoming experiments. Note that these curves include uncertainties associated with the instrumental beam. The red line shows the B-mode power spectrum for the standard inflationary model with $r = 0.1$.

$$N_l^X = \left(\sum_c \frac{1}{N_{l,c}^X} \right)^{-1}, \tag{1.12}$$

where the noise spectrum of an individual frequency channel, assuming a Gaussian beam, is

$$N_{l,c}^X = (\sigma_{\rm pix}\, \theta_{\rm fwhm})^2 \exp\left[l(l+1) \frac{\theta_{\rm fwhm}^2}{8 \ln 2} \right] \delta_{XY}. \tag{1.13}$$

The pixel noise from temperature and polarisation maps are considered as uncorrelated. The noise per pixel $\sigma_{\rm pix}^X$ (and $\sigma_{\rm pix}^P = \sqrt{2}\sigma_{\rm pix}^T$) depends on the instrumental parameters; $\theta_{\rm fwhm}$ is the *full width at half maximum* (FHWM) of the Gaussian beam.

For the Planck experiment, we include three channels with frequencies (100 GHz, 143 GHz, 217 GHz) and noise levels per beam $(\sigma_{\rm pix}^T)^2$= (46.25 μK^2, 36 μK^2, 171 μK^2). The FHWM of the three channels are $\theta_{\rm fwhm}$ =(9.5, 7.1, 5.0) arc-minute. These figures are taken from the values given in [52]. We combine three channels for the CMBPol experiment [5] with frequencies (100 GHz, 150 GHz, 220 GHz), noise levels $(\sigma_{\rm pix}^T)^2$ = (729 nK^2, 676 nK^2, 1600 nK^2) and $\theta_{\rm fwhm}$ = (8, 5, 3.5) arc-minute. Sky coverages of $f_{\rm sky} = 0.65, 0.8$ are respectively assumed and integration time of 14 months. In Figure 1.9, we show the noise levels for these experiments as a function of multipole number l. The blue line corresponds to the B-mode power spectrum using the standard power-law parameterisation with $r = 0.1$. The lensed C_l^B is also shown in the same figure, which can be treated as a part of the total noise power spectrum N_l^B as well as the instrumental noise power spectra [51]. For more information of the noise and beam profile of each frequency channel, refer to [42].

1.3 Bayesian Analysis

Over the last decade or so, the vast amount of information coming from a wide range of sources, including CMB, SNe and LSS, has increased amazingly. We would like to translate this experimental/observational information into constraints of our model(s), summarised by the estimation of the cosmological parameters involved. The concordance ΛCDM model, previously described, depends on a set of cosmological parameters shown in Section 1.1. A primary goal concerning observational cosmology is to determine best-fit parameter values for a given model, as well as to decide which model is in best-agreement with observational data. To do this we focus on *Bayesian inference*. Some excellent reviews of Bayesian statistics applied to cosmology are given by Heavens [21], Liddle [39], Liddle et al. [41], Verde [67, 68], von Toussaint [69**?**], and the textbook for data analysis Sivia and Skilling [61].

1.3.1 Parameter estimation

A Bayesian analysis provides a consistent approach to estimating the values of the parameters $\mathbf{\Theta}$ within a model M, which best describe the data $\mathbf{D}$. The method is based on the assignment of probabilities to the quantities of interest, and then the manipulation of these probabilities given a series of rules, in which Bayes' theorem plays the main role [39]. Bayes' theorem states that

$$P(\mathbf{\Theta}|\mathbf{D}, M) = \frac{P(\mathbf{D}|\mathbf{\Theta}, M)\ P(\mathbf{\Theta}|M)}{P(\mathbf{D}|M)}. \tag{1.14}$$

In this expression, the *prior* probability $\mathrm{P}(\mathbf{\Theta}|\mathrm{M}) \equiv \pi$ represents what we thought the probability of $\mathbf{\Theta}$ was before considering the data. This probability is modified through the *likelihood* $\mathrm{P}(\mathbf{D}|\mathbf{\Theta},\mathrm{M}) \equiv \mathcal{L}$. The posterior probability $\mathrm{P}(\mathbf{\Theta}|\mathbf{D},\mathrm{M})$ represents the state of knowledge once we have taken the experimental data $\mathbf{D}$ into account. The normalisation constant in the denominator is the marginal likelihood or *Bayesian evidence* $\mathrm{P}(\mathbf{D}|\mathrm{M}) \equiv \mathcal{Z}$, as is normally called in cosmology. Since this quantity is independent of the parameters $\mathbf{\Theta}$, it is commonly ignored in parameter estimation but it takes the central role for model comparison.

The central step for parameter estimation is to construct the likelihood function $\mathcal{L}$ for the measurements, and then the exploration of the region around its maximum value $\mathcal{L}_{\max}$. A simple chi-squared function is often used $\chi^2 = -2\ln\mathcal{L}$. when the distributions are Gaussian. However, some current problems in cosmology present obstacles for carrying out this procedure

straightforwardly (some of them discussed by Liddle [39]). Fortunately, models of our interest can be easily tackled by numerical techniques developed on statistical fields, in particular the methods known as *Markov Chain Monte Carlo (MCMC)*. There have been developed different codes employing MCMC techniques to carry out the exploration of the cosmological parameter-space, for instance CosmoMC [36], CosmoHammer [2], CMBEASY [14]. Although some of them use a simple Metropolis-Hasting algorithm by default, nowadays improved algorithms have been adapted to explore complex posterior probability distributions.

Discriminating among models and determining which of them is the most plausible given some data is a task for model comparison techniques, whose application is discussed in the next section.

1.3.2 Model selection

There is nowadays a rich diversity of models trying to describe the vast amount of cosmological information. Some of them might involve complex interactions or introduce a high number of parameters, but provide just as good fit as the standard ΛCDM model (see Table 1.1). So, how can we perform an objective comparison between them and choose the appropriate model?. The solution was proposed by William of Occam: the simplest model which covers all the facts ought to be preferred. That is, a complex model that explains the data slightly better than a simple one should be penalised by the inclusion of extra parameters, because this additional information reflects a lack of predictability in the model. Moreover, if a model is too simple, it might not fit certain data equally well, then it can be discarded [41**?**].

Many attempts have been performed to translate Occam's razor into a mathematical language for model selection. Two major types have been used so far: Bayesian evidence and *Information criteria*; where the latter one can be used as an useful approximation when the Bayesian evidence cannot be computed.

Information criteria is based on some simplifying approximations to the full Bayesian evidence. The method considers the best-fit values and attaches a penalty term for more complex models:

- The Akaike Information criterion (AIC), introduced by Hirotugu Akaike has the form

$$AIC \equiv -2 \ln \mathcal{L}_{max} + 2k, \tag{1.15}$$

where the penalty term is induced by the number of free parameters k to be estimated.

- The Bayesian Information Criterion (BIC), was derived by Gideon E. Schwarz and it is given by

$$BIC \equiv -2 \ln \mathcal{L}_{max} + k \ln N, \tag{1.16}$$

where N is the number of datapoints. It follows from a Gaussian approximation of the Bayesian evidence for a large number of samples.

- The Deviance Information Criterion (DIC), was proposed by David J Spiegelhalter. It is a generalization of the AIC and BIC written as

$$DIC \equiv -2\widehat{D_{KL}} + 2\mathcal{C}_b, \tag{1.17}$$

where the former term is the estimated KL divergence and the latter one is the effective number of parameters.

An extended discussion of the different information criteria can be found in [38, 41**?**].

Bayesian evidence. This is the primordial tool for the model selection we focus on. It applies the same type of analysis as in parameter estimation, but now at the level of models rather than parameters. The Bayesian evidence is the key quantity to bear in mid as it balances the complexity of cosmological models and then, naturally, incorporates Occam's razor. It has been applied to a wide diversity of cosmological contexts, see for example [24, 27**?**].

Let us consider several models M, each of them with prior probability $P(M)$. Bayes' theorem for model selection is

$$P(M|\mathbf{D}) = \frac{P(\mathbf{D}|M)P(M)}{P(\mathbf{D})}. \tag{1.18}$$

The left-hand side denotes the probability of the model given the data, which is exactly what we are looking for in model selection. We need, therefore, to obtain an expression that allows us to compute the Bayesian evidence in terms of the information we already have. As we previously mentioned, the Bayesian evidence is simply the normalisation constant of the posterior distribution expressed by

$$\mathcal{Z} = \int \mathcal{L}(D|\Theta)\pi(\Theta)d^N\Theta. \tag{1.19}$$

Table 1.2: Jeffreys guideline scale for evaluating the strength of evidence when two models are compared.

$\lvert\mathcal{B}_{i,j}\rvert$	Odds	Probability	Strength
< 1.0	$< 3:1$	< 0.750	Inconclusive
1.0-2.5	$\sim 12:1$	0.923	Significant
2.5-5.0	$\sim 150:1$	0.993	Strong
> 5.0	$> 150:1$	> 0.993	Decisive

where N is the dimensionality of the parameter space. More explicitly, it is the average likelihood weighted by the prior for a specific model choice:

$$Evidence = \int (Likelihood \times Prior) d^N\Theta. \tag{1.20}$$

A model containing wider regions of prior parameter-space along with higher likelihoods will have a high evidence and vice versa. Therefore, the Bayesian evidence does provide a natural mechanism to balance the complexity of cosmological models and then, elegantly incorporates Occam's razor.

When comparing two models, M_i and M_j, the important quantity to bear in mind is the ratio of the posterior probabilities, or *posterior odds*, given by

$$\frac{P(M_i|\mathbf{D})}{P(M_j|\mathbf{D})} = \frac{\mathcal{Z}_i}{\mathcal{Z}_j}\frac{P(M_i)}{P(M_j)}, \tag{1.21}$$

where $P(M_i)/P(M_j)$ is the prior probability ratio for the two models, usually set to unity. The ratio of two evidences $\mathcal{Z}_i/\mathcal{Z}_j$ (or equivalently the difference in log evidences $\ln \mathcal{Z}_i - \ln \mathcal{Z}_j$) is often termed the *Bayes factor* $\mathcal{B}_{i,j}$:

$$\mathcal{B}_{i,j} = \ln \frac{\mathcal{Z}_i}{\mathcal{Z}_j}. \tag{1.22}$$

Then, the quantity $\mathcal{B}_{i,j}$ measures the relative probability of how well model i may fit the data when is compared to model j. Jeffreys [26] provided a suitable guideline scale on which we are able to make qualitative conclusions (see Table 1.2). In this work, we refer to positive (negative) values of $\mathcal{B}_{i,j}$ when the i model being favoured (disfavoured) over model j.

The calculation of the integral in Equation (1.19) is a very computationally demanding process, since it requires a multidimensional integration over the likelihood and prior. For many years much progress has been made in the construction of efficient algorithms to allow faster and more accurate computation of the Bayesian evidence. Until recently, algorithms such as simulating annealing or thermodynamic integration [8], required around 10^7 likelihood evaluations making the procedure hardly treatable. A powerful algorithm was recently invented by Skilling [62], known as *nested sampling algorithm*, which has been proven to be ten times more efficient than previous methods. The first computationally-efficient code to compute the Bayesian evidence in cosmology, named CosmoNest, was implemented by Mukherjee et al. [48]. In this work we incorporate into the CosmoMC software [36] a substantially improved and fully-parallelized version of the *nested sampling* algorithm, called the MultiNest algorithm, initially proposed by Feroz & Hobson [17, 18]. The MultiNest algorithm increases the sampling efficiency for calculating the evidence and allows one to obtain posterior samples even from distributions with multiple modes and/or pronounced degeneracies between parameters. There is also CosmoPMC which is based on an adaptative importance sampling method called Population Monte Carlo [30]. For more complex models with high number of parameters, there also exist improved codes to increase the speed of the whole process by employing, for instance, neuronal networks: CosmoNet [4]. BAMBI is an algorithm that combines the benefits of both the nested sampling and artificial neural networks [20].

1.3.3 Dataset consistency

Combining multiple datasets to obtain tight constraints on the cosmological parameters has been a very common practice. Marshall et al. [44] established a test to quantify the consistency of different cosmological datasets analysed under the same model (see also Hobson et al. [25]). The Bayesian consistency analysis relies on partitioning the full combined dataset D into its constituent parts D_i ($i = 1, \ldots, n$), namely CMB, SNe, LSS data, so on, and analyses the model with each dataset independently. The evidence ratio is defined as

$$R = \frac{\Pr(D|H)}{\prod_{i=1}^{n} \Pr(D_i|H)}, \tag{1.23}$$

where the hypothesis H denotes the model under study. This ratio compares the probability that all the datasets were generated from a cosmological model characterised by the same parameter values, with the probability that each dataset was generated from an independent

Parameters	Description	Prior range
Background		
$\Omega_{\rm b,0}h^2$	Physical baryon density	$[0.01, 0.03]$
$\Omega_{\rm dm,0}h^2$	Physical cold dark matter density	$[0.01, 0.3]$
θ	Ratio of the sound horizon to the angular diameter distance	$[1, 1.1]$
τ	Reionization optical depth	$[0.01, 0.3]$
Inflationary		
$\log[10^{10}A_{\rm s}]$	Curvature perturbation amplitude	$[2.5, 4]$
$n_{\rm s}$	Spectral scalar index	$[0.5, 1.2]$
Secondary		
$A_{\rm SZ}$	Sunyaev-Zel'dovich amplitude	$[0, 3]$
$A_{\rm c}$	Total Poisson power	$[0, 20]$
$A_{\rm p}$	Amplitude of the clustered power	$[0, 30]$

Table 1.3: Parameter description along with the flat-uniform priors assumed on the standard ΛCDM.

set of cosmological parameters. Thus, one expects $R > 1$ if the datasets are all consistent, and $R < 1$ otherwise. The Bayes factor for data sets is given by $\mathcal{B}_R = \ln R$.

1.4 The concordance ΛCDM model

In this section, we make use of the theoretical (Section 1.1), Observational (Section 1.2.1) and Statistical (Section 1.3) tools to examine the standard cosmological model. The minimal form of the standard cosmological model, in agreement with several independent observations, considers a FRW background, purely Gaussian adiabatic scalar perturbations and neglect tensor contributions. It also assumes a flat universe fill up with baryons, cold dark matter and a dark energy component in the form of a cosmological constant Λ. The key aspects that describe the standard model here, and throughout the work, are specified by:

- Theory/Parameters

Base parameters: the physical baryon and dark matter densities $\Omega_{\rm b,0}h^2$ and $\Omega_{\rm dm,0}h^2$, $100\times$ the ratio of the sound horizon to angular diameter distance at last scattering surface θ, the optical depth at reionisation τ, the amplitude of the primordial spectrum $A_{\rm s}$ and the spectral index $n_{\rm s}$ defined at a pivot scale $k_0 = 0.002$ Mpc^{-1}. Aside from the base parameters, recent observations include additional secondary parameters: the Sunyaev-Zel'dovich (SZ) amplitude

A_{SZ}, the total Poisson power A_p at $l = 3000$ and the amplitude of the clustered power A_c. The parameters, along with the flat priors, are shown in Table 1.3.

-Observations/Experiments:

To compute posterior probabilities for each model in the light of temperature and polarisation measurements, we use WMAP 7-year data release [31] and the ACT observations [15]. In addition to CMB data, we include distance measurements of 557 Supernovae Type Ia from the Union 2 compilation [33]. We also incorporate large-scale structure data from the SDSS-DR7 [54] power spectrum. We consider baryon density information from BBN [10] and impose a Gaussian prior on H_0 using measurements from the HST [56]. This compromises our dataset I. In addition to dataset I, we include recent results from QUaD [9] and BICEP [11] experiments. Together these observations make up our dataset II.

-Analysis/Codes:

The computation of the CMB spectrum is perform by a modified version of the CAMB code [37] to include any additional components and calculate the predicted power spectra of CMB anisotropies and matter perturbations. The exploration of the parameter-space is carried out by using the CosmoMC software [36] with the addition of the Multinest algorithm [17]. The latter is included to the perform the calculation of the Bayesian evidence.

We have analysed a standard flat ΛCDM model and, for pedagogical purposes, also the same model but with the addition of curvature, with priors $\Omega_{k,0} = [-0.1, 0.1]$. The top panel of Figure 1.10 shows 1D marginalised posterior distributions of the base and some relevant derived parameters, for both models: flat and non-flat ΛCDM. At the top of the same figure, we have included the Bayes factor comparing both of them. For the non-flat model, we notice that the marginalised posteriors of $\Omega_{\mathrm{dm},0}h^2$, H_0 and the Age of the universe have broadened due to correlations created by the inclusion of $\Omega_{k,0}$. These correlations can be observed in the 2D marginalised posterior distribution shown in the bottom panel of Figure 1.10. The constraints on the cosmological parameters are displayed in Table 1.4 along with 1σ confidence levels. In this Table, both models assume the presence of ΛCDM with a scalar power spectrum described by a power-law and no tensor contributions. The first set of rows show the base parameters whereas the second set some derived parameters. Current cosmological observations provide, in general terms, a strong support for a nearly-flat accelerating universe dominated by 72% of

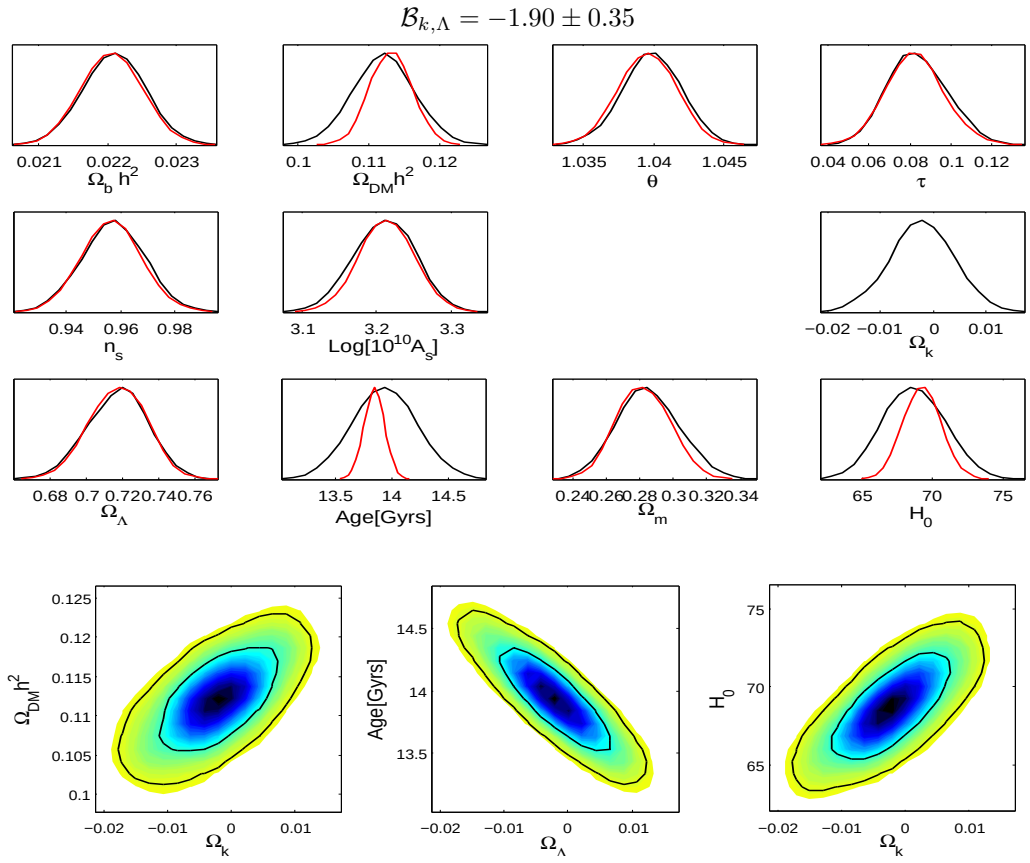

Figure 1.10: Top: 1D marginalised posterior distributions on the standard ΛCDM parameters using current cosmological observations. Bottom: 2D marginalised posterior distributions of non-flat ΛCDM parameters; constraints are plotted with 1σ and 2σ confidence contours.

dark energy in the form of a cosmological constant, 24% of non-baryonic dark matter and 4% of baryon contributions; the primordial spectrum is red ($n_s < 1$) with the Harrison-Zel'dovich excluded with high confidence level. On the other hand, the Bayes factor between these two models, $\mathcal{B}_{\Lambda,\Lambda+\Omega_k} = +1.90 \pm 0.35$, indicates a significant preference for a flat universe, according to the Jeffreys guideline. The last row of Table 1.4 shows that both models are consistent with the full combined dataset I.

Throughout the rest of the chapters we incorporate features beyond the standard ΛCDM model in the search of a better description of cosmological observations. In Chapter **??**, with the use of present data, we determine the structure of the primordial scalar spectrum by implementing an optimal model-free reconstruction. Our aim is to consider models that slightly

Table 1.4: The constraints on the cosmological parameters using our dataset II. We report the mean of the marginalised posterior distribution and 1σ confidence levels. The Bayes factor for models $\mathcal{B}_{\Lambda,\Lambda+\Omega_k}$, and for datasets $\mathcal{B}_R$ are also included.

Description		Flat ΛCDM	Non-flat ΛCDM
Base parameters	$\Omega_{\rm b,0}h^2$	0.02206 ± 0.00042	0.0221 ± 0.00043
	$\Omega_{\rm dm,0}h^2$	0.1130 ± 0.0028	0.112 ± 0.0041
	θ	1.039 ± 0.0019	1.039 ± 0.0020
	τ	0.082 ± 0.013	0.083 ± 0.014
	$n_{\rm s}$	0.956 ± 0.010	0.957 ± 0.011
	$\log[10^{10}A_{\rm s}]$	3.21 ± 0.035	3.21 ± 0.039
	$\Omega_{k,0}$	-	-0.0022 ± 0.0058
Derived parameters	$\Omega_{\rm m,0}$	0.282 ± 0.015	0.285 ± 0.018
	$\Omega_{\Lambda,0}$	0.717 ± 0.015	0.717 ± 0.016
	H_0	69.2 ± 1.27	68.7 ± 2.13
	Age(Gyrs)	13.84 ± 0.086	13.93 ± 0.27
Bayes factor	$-2\ln\mathcal{L}_{\rm max}$	8240.46	8240.80
	$\mathcal{B}_{\Lambda,\Lambda+\Omega_k}$	$+1.6 \pm 0.4$	-
Dataset consistency	$\mathcal{B}_R$	$+5.06 \pm 0.4$	$+5.07 \pm 0.4$

deviate from the simple power-law form. Then, in Chapter **??**, we incorporate tensor contributions to the analysis and present current and future constraints on the scalar spectrum. Chapter **??** explores the possibility of a dynamical behaviour of dark energy. Here, the dark energy equation-of-state $w_{\rm de}(z)$ is modelled as a linear interpolation between a set of 'nodes' with varying amplitudes and redshifts, similarly to the approach used in Chapter **??**. In the search of mechanisms or candidates to explain the mild time-dependence of $w_{\rm de}(z)$, in Chapter **??** we remain focussed on the ΛCDM model but now include a second dark energy component Ω_X with equation-of-state w_X. Finally, in Chapter **??** the Einstein-Hilbert Lagrangian is considered as a limit case of a more general form of it, namely Modified Gravity. We explore these models as an alternative to the dark energy component. The summary of the work done throughout this dissertation is sketched in Figure 1.11.

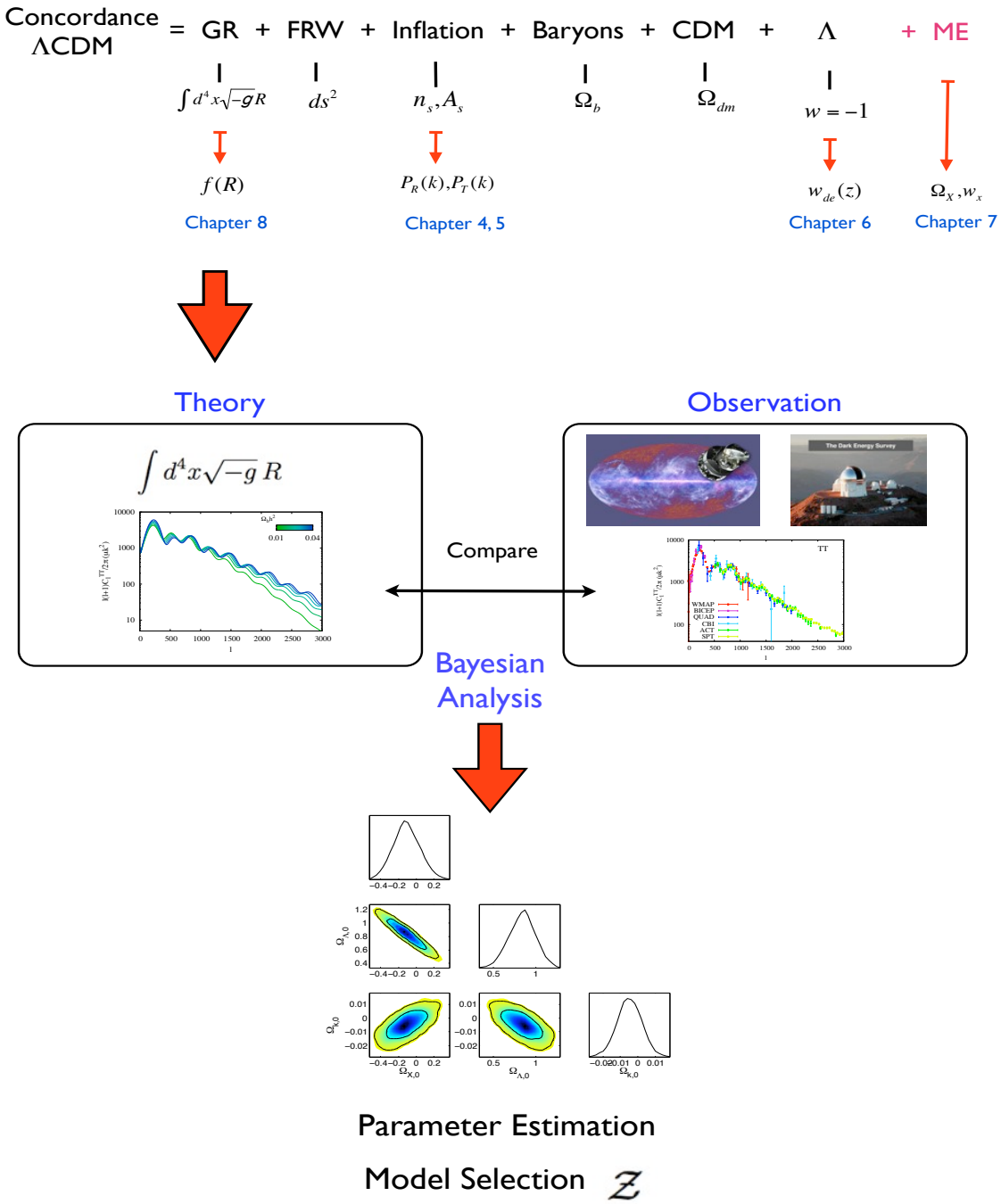

Figure 1.11: Summary of the work performed throughout this dissertation. The top panel of the Figure displays the features beyond the concordance ΛCDM model considered through the following chapters.

Bibliography

[1] Christopher P. Ahn et al. The Ninth Data Release of the Sloan Digital Sky Survey: First Spectroscopic Data from the SDSS-III Baryon Oscillation Spectroscopic Survey. Astrophys.J.Suppl., 203:21, 2012. doi: 10.1088/0067-0049/203/2/21.

[2] Joel Akeret, Sebastian Seehars, Adam Amara, Alexandre Refregier, and Andre Csillaghy. CosmoHammer: Cosmological parameter estimation with the MCMC Hammer. 2012. [arXiv:1212.1721].

[3] R. Amanullah and *et. al.* Spectra and Hubble Space Telescope Light Curves of Six Type Ia Supernovae at $0.511 < z < 1.12$ and the Union2 Compilation. The Astrophysical Journal, 716(1):712, 2010. URL http://stacks.iop.org/0004-637X/716/i=1/a=712.

[4] T. Auld, M. Bridges, and M. P. Hobson. Cosmonet: fast cosmological parameter estimation in non-flat models using neural networks. Monthly Notices of the Royal Astronomical Society, 387(4):1575–1582, 2008. doi: 10.1111/j.1365-2966.2008.13279.x. URL http://mnras.oxfordjournals.org/content/387/4/1575.abstract.

[5] B-Pol Collaboration.*http://www.b-pol.org/documents.php*, 2010.

[6] M. Bowden and et. al. Scientific optimization of a ground-based CMB polarization experiment. Monthly Notices of the Royal Astronomical Society, 349(1):321–335, 2004. ISSN 1365-2966. doi: 10.1111/j.1365-2966.2004.07506.x. URL http://dx.doi.org/10.1111/j.1365-2966.2004.07506.x.

[7] D Branch and G A Tammann. Type Ia Supernovae as Standard Candles. Annual Review of Astronomy and Astrophysics, 30(1):359–389, 1992. doi: 10.1146/annurev.aa.30.

090192.002043. URL http://www.annualreviews.org/doi/abs/10.1146/annurev.aa.30.090192.002043.

[8] M. Bridges, A. N. Lasenby, and M. P. Hobson. A Bayesian analysis of the primordial power spectrum. Monthly Notices of the Royal Astronomical Society, 369(3):1123–1130, 2006. ISSN 1365-2966. doi: 10.1111/j.1365-2966.2006.10351.x. URL http://dx.doi.org/10.1111/j.1365-2966.2006.10351.x.

[9] M. L. Brown and et. al. Improved Measurements of the Temperature and Polarization of the Cosmic Microwave Background from QUaD. The Astrophysical Journal, 705(1):978, 2009. URL http://stacks.iop.org/0004-637X/705/i=1/a=978.

[10] Scott Burles, Kenneth M. Nollett, and Michael S. Turner. Big Bang Nucleosynthesis Predictions for Precision Cosmology. The Astrophysical Journal Letters, 552(1):L1, 2001. URL http://stacks.iop.org/1538-4357/552/i=1/a=L1.

[11] H. C. Chiang and et. al. Measurement of Cosmic Microwave Background Polarization Power Spectra from Two Years of BICEP Data. The Astrophysical Journal, 711(2):1123, 2010. URL http://stacks.iop.org/0004-637X/711/i=2/a=1123.

[12] Marina Cortês, Andrew R. Liddle, and David Parkinson. On the prior dependence of constraints on the tensor-to-scalar ratio. Journal of Cosmology and Astroparticle Physics, 2011(09):027, 2011. URL http://stacks.iop.org/1475-7516/2011/i=09/a=027.

[13] B. P. Crill and *et. al.* SPIDER: a balloon-borne large-scale CMB polarimeter. Proc. SPIE 7010, Space Telescopes and Instrumentation 2008, pages 70102P–70102P–12, 2008. doi: 10.1117/12.787446. URL +http://dx.doi.org/10.1117/12.787446.

[14] Michael Doran. CMBEASY: an object oriented code for the cosmic microwave background. Journal of Cosmology and Astroparticle Physics, 2005(10):011, 2005. URL http://stacks.iop.org/1475-7516/2005/i=10/a=011.

[15] J. Dunkley and *et. al.* The Atacama Cosmology Telescope: Cosmological Parameters from the 2008 Power Spectra. [arXiv:1009.0866], 2010. URL http://arxiv.org/abs/1009.0866v1.

[16] Euclid Missin Consortium.*http://www.euclid-ec.org/*, 2012.

[17] F. Feroz and M. P. Hobson. Multimodal nested sampling: an efficient and robust alternative to Markov Chain Monte Carlo methods for astronomical data analyses. Monthly Notices of the Royal Astronomical Society, 384(2):449–463, 2008. ISSN 1365-2966. doi: 10.1111/j.1365-2966.2007.12353.x. URL http://dx.doi.org/10.1111/j.1365-2966.2007.12353.x.

[18] F. Feroz, M. P. Hobson, and M. Bridges. MultiNest: an efficient and robust Bayesian inference tool for cosmology and particle physics. Monthly Notices of the Royal Astronomical Society, 398(4):1601–1614, 2009. ISSN 1365-2966. doi: 10.1111/j.1365-2966.2009.14548.x. URL http://dx.doi.org/10.1111/j.1365-2966.2009.14548.x.

[19] Joshua A. Frieman and *et. al.* The Sloan Digital Sky Survey-II Supernova Survey: Technical Summary. The Astronomical Journal, 135(1):338, 2008. URL http://stacks.iop.org/1538-3881/135/i=1/a=338.

[20] Philip Graff, Farhan Feroz, Michael P. Hobson, and Anthony Lasenby. BAMBI: blind accelerated multimodal Bayesian inference. Monthly Notices of the Royal Astronomical Society, 421(1):169–180, 2012. doi: 10.1111/j.1365-2966.2011.20288.x. URL http://mnras.oxfordjournals.org/content/421/1/169.abstract.

[21] Alan Heavens. Statistical techniques in cosmology. [arXiv:0906.0664], 2010.

[22] G. Hinshaw and *et. al.* Nine-Year Wilkinson Microwave Anisotropy Probe (WMAP) Observations: Cosmological Parameter Results. [arXiv:1212.5226], 2013.

[23] R. Hlozek and *et. al.* The Atacama Cosmology Telescope: a measurement of the primordial power spectrum. [arXiv:1105.4887], 2011. URL http://arxiv.org/abs/1105.4887v1.

[24] M. P. Hobson and C. McLachlan. A Bayesian approach to discrete object detection in astronomical data sets. Monthly Notices of the Royal Astronomical Society, 338(3):765–784, 2003. ISSN 1365-2966. doi: 10.1046/j.1365-8711.2003.06094.x. URL http://dx.doi.org/10.1046/j.1365-8711.2003.06094.x.

[25] M. P. Hobson, S. L. Bridle, and O Lahav. Combining cosmological data sets: hyperparameters and bayesian evidence. Monthly Notices of the Royal Astronomical Society, 335(2):377–388, 2002. ISSN 1365-2966. doi: 10.1046/j.1365-8711.2002.05614.x. URL http://dx.doi.org/10.1046/j.1365-8711.2002.05614.x.

[26] Harold Jeffreys. Theory of Probability. Oxford University Press, 1998.

[27] Moncy V. John and J. V. Narlikar. Comparison of cosmological models using Bayesian theory. Phys. Rev. D, 65:043506, Jan 2002. doi: 10.1103/PhysRevD.65.043506. URL http://link.aps.org/doi/10.1103/PhysRevD.65.043506.

[28] W. C. Jones and *et. al.* A Measurement of the Angular Power Spectrum of the CMB Temperature Anisotropy from the 2003 Flight of BOOMERANG. The Astrophysical Journal, 647(2):823, 2006. URL http://stacks.iop.org/0004-637X/647/i=2/a=823.

[29] R. Keisler and *et. al.* A Measurement of the Damping Tail of the Cosmic Microwave Background Power Spectrum with the South Pole Telescope. [arXiv:1105.3182], 2011. URL http://arxiv.org/abs/1105.3182v2.

[30] Martin Kilbinger, Karim Benabed, Olivier Cappe, Jean-Francois Cardoso, Gersende Fort, et al. CosmoPMC: Cosmology Population Monte Carlo. arXiv:1101.0950, 2011.

[31] E. Komatsu and *et. al.* Seven-year Wilkinson Microwave Anisotropy Probe (WMAP) Observations: Cosmological Interpretation. The Astrophysical Journal Supplement Series, 192(2):18, 2011. URL http://stacks.iop.org/0067-0049/192/i=2/a=18.

[32] Arthur Kosowsky, Milos Milosavljevic, and Raul Jimenez. Efficient cosmological parameter estimation from microwave background anisotropies. Phys. Rev. D, 66:063007, Sep 2002. doi: 10.1103/PhysRevD.66.063007. URL http://link.aps.org/doi/10.1103/PhysRevD.66.063007.

[33] M. Kowalski and *et. al.* Improved Cosmological Constraints from New, Old, and Combined Supernova Data Sets. The Astrophysical Journal, 686(2):749, 2008. URL http://stacks.iop.org/0004-637X/686/i=2/a=749.

[34] Ofer Lahav and Andrew R Liddle. The Cosmological Parameters 2010. 2010. [arXiv:1207.4898].

[35] D. Larson and *et. al.* Seven-year Wilkinson Microwave Anisotropy Probe (WMAP) Observations: Power Spectra and WMAP-derived Parameters. The Astrophysical Journal Supplement Series, 192(2):16, 2011. URL http://stacks.iop.org/0067-0049/192/i=2/a=16.

[36] Antony Lewis and Sarah Bridle. Cosmological parameters from CMB and other data: A Monte Carlo approach. Physical Review D, 66(10), 2002. doi: 10.1103/PhysRevD.66.103511.

[37] Antony Lewis, Anthony Challinor, and Anthony Lasenby. Efficient Computation of Cosmic Microwave Background Anisotropies in Closed Friedmann-Robertson-Walker Models. The Astrophysical Journal, 538(2):473, 2000. URL http://stacks.iop.org/0004-637X/538/i=2/a=473.

[38] Andrew R. Liddle. How many cosmological parameters? Monthly Notices of the Royal Astronomical Society, 351(3):L49–L53, 2004. ISSN 1365-2966. doi: 10.1111/j.1365-2966.2004.08033.x. URL http://dx.doi.org/10.1111/j.1365-2966.2004.08033.x.

[39] Andrew R. Liddle. Statistical Methods for Cosmological Parameter Selection and Estimation. Annual Review of Nuclear and Particle Science, 59(1):95–114, 2009. doi: 10.1146/annurev.nucl.010909.083706. URL http://www.annualreviews.org/doi/abs/10.1146/annurev.nucl.010909.083706.

[40] Andrew R. Liddle and David H. Lyth. COBE, gravitational waves, inflation and extended inflation. Physics Letters B, 291(4):391 – 398, 1992. ISSN 0370-2693. doi: 10.1016/0370-2693(92)91393-N. URL http://www.sciencedirect.com/science/article/pii/037026939291393N.

[41] Andrew R. Liddle, Pia Mukherjee, and David Parkinson. Cosmological model selection. [arXiv:0608184], 2006.

[42] Yin-Zhe Ma, Wen Zhao, and Michael L. Brown. Constraints on standard and non-standard early universe models from CMB B -mode polarization. Journal of Cosmology and Astroparticle Physics, 2010(10):007, 2010. URL http://stacks.iop.org/1475-7516/2010/i=10/a=007.

[43] M. C. March, N. V. Karpenka, F. Feroz, and M. P. Hobson. Comparison of cosmological parameter inference methods applied to supernovae lightcurves fitted with SALT2. [arXiv:1207.3705], 2012.

[44] Phil Marshall, Nutan Rajguru, and An že Slosar. Bayesian evidence as a tool for comparing datasets. Phys. Rev. D, 73:067302, Mar 2006. doi: 10.1103/PhysRevD.73.067302. URL http://link.aps.org/doi/10.1103/PhysRevD.73.067302.

[45] J. C. Mather and *et. al.* Calibrator design for the cobe far infrared absolute spectrophotometer (firas). The Astrophysical Journal, 512(2):511, 1999. URL http://stacks.iop.org/0004-637X/512/i=2/a=511.

[46] Patrick McDonald, Uroš Seljak, Scott Burles, and et al. The lya forest power spectrum from the sloan digital sky survey. The Astrophysical Journal Supplement Series, 163(1): 80, 2006. URL http://stacks.iop.org/0067-0049/163/i=1/a=80.

[47] G. Miknaitis and *et. al.* The ESSENCE Supernova Survey: Survey Optimization, Observations, and Supernova Photometry. The Astrophysical Journal, 666(2):674, 2007. URL http://stacks.iop.org/0004-637X/666/i=2/a=674.

[48] Pia Mukherjee, David Parkinson, and Andrew R. Liddle. A Nested Sampling Algorithm for Cosmological Model Selection. The Astrophysical Journal Letters, 638(2):L51, 2006. URL http://stacks.iop.org/1538-4357/638/i=2/a=L51.

[49] Paul Oxley, Peter A. Ade, and et al. The EBEX experiment. Proc. SPIE 5543, Infrared Spaceborne Remote Sensing XII, pages 320–331, 2004. doi: 10.1117/12.563447. URL +http://dx.doi.org/10.1117/12.563447.

[50] S. Perlmutter, G. Aldering, G. Goldhaber, and et al. Measurements of Ω and Λ from 42 High-Redshift Supernovae. The Astrophysical Journal, 517(2):565, 1999. URL http://stacks.iop.org/0004-637X/517/i=2/a=565.

[51] Laurence Perotto, Julien Lesgourgues, Steen Hannestad, Huitzu Tu, and Yvonne Y Y Wong. Probing cosmological parameters with the CMB: forecasts from Monte Carlo simulations. Journal of Cosmology and Astroparticle Physics, 2006(10):013, 2006. URL http://stacks.iop.org/1475-7516/2006/i=10/a=013.

[52] Planck Collaboration. The Science Programme of Planck. [astro-ph/0604069], 2012.

[53] Brian A. Powell. Tensor tilt from primordial b-modes. [arXiv:1106.5059], 2011.

[54] Beth A. Reid and *et. al.* Cosmological constraints from the clustering of the Sloan Digital Sky Survey DR7 luminous red galaxies. Monthly Notices of the Royal Astronomical Society, 404(1):60–85, 2010. ISSN 1365-2966. doi: 10.1111/j.1365-2966.2010.16276.x. URL http://dx.doi.org/10.1111/j.1365-2966.2010.16276.x.

[55] Adam G. Riess and *et. al.* New Hubble Space Telescope Discoveries of Type Ia Supernovae at $z \geq 1$ Narrowing Constraints on the Early Behavior of Dark Energy. The Astrophysical Journal, 659(1):98, 2007. URL http://stacks.iop.org/0004-637X/659/i=1/a=98.

[56] Adam G. Riess and *et. al.* A Redetermination of the Hubble Constant with the Hubble Space Telescope from a Differential Distance Ladder. The Astrophysical Journal, 699(1): 539, 2009. URL http://stacks.iop.org/0004-637X/699/i=1/a=539.

[57] Adam G. Riess, Alexei V. Filippenko, Peter Challis, and et al. Observational evidence from supernovae for an accelerating universe and a cosmological constant. The Astronomical Journal, 116(3):1009, 1998. URL http://stacks.iop.org/1538-3881/116/i=3/a=1009.

[58] J.A. Rubino-Martin, R. Rebolo, M. Tucci, R. Genova-Santos, S.R. Hildebrandt, et al. The Quijote CMB Experiment. 2008. arXiv:0810.3141.

[59] Sievers and *et. al.* The Atacama Cosmology Telescope: Cosmological parameters from three seasons of data. [arXiv: 1301.0824], 2013.

[60] J. L. Sievers and *et. al.* Cosmological Parameters from Cosmic Background Imager Observations and comparisons with boomerang, dasi, and maxima. The Astrophysical Journal, 591(2):599, 2003. URL http://stacks.iop.org/0004-637X/591/i=2/a=599.

[61] Devinderjit Sivia and John Skilling. Data Analysis: A Bayesian Tutorial. OUP Oxford, 2006.

[62] J. Skilling. Nested sampling for general Bayesian computation. Bayesian Analysis, 1(4): 833–860, 2006.

[63] K. T. Story and *et. al.* A Measurement of the Cosmic Microwave Background Damping Tail from the 2500-square-degree SPT-SZ survey. [arXiv:1210.7231], 2012.

[64] M. Sullivan and *et. al.* SNLS3: Constraints on Dark Energy Combining the Supernova Legacy Survey Three-year Data with Other Probes. The Astrophysical Journal, 737(2): 102, 2011. URL http://stacks.iop.org/0004-637X/737/i=2/a=102.

[65] N. Suzuki and *et. al.* The Hubble Space Telescope Cluster Supernova Survey. V. Improving the Dark-energy Constraints above $z > 1$ and Building an Early-type-hosted Supernova Sample. The Astrophysical Journal, 746(1):85, 2012. URL http://stacks.iop.org/0004-637X/746/i=1/a=85.

[66] The Dark Energy Survey.*http://www.darkenergysurvey.org/index.shtml*, 2012.

[67] Licia Verde. A practical guide to Basic Statistical Techniques for Data Analysis in Cosmology. [arXiv:0712.3028], 2008.

[68] Licia Verde. Statistical methods in cosmology. [arXiv:0911.3105], 2009.

[69] Udo von Toussaint. Bayesian inference in physics. Rev. Mod. Phys., 83:943–999, Sep 2011. doi: 10.1103/RevModPhys.83.943. URL http://link.aps.org/doi/10.1103/RevModPhys.83.943.